AD-A132234

AD A 132 234

AD-E401 065

TECHNICAL REPORT ARLCD-TR-83033

N(2) AND CO VIBRATIONAL CARS AND H(2) ROTATIONAL CARS SPECTROSCOPY OF CH(4)-N(2)O FLAMES

KENNETH ARON
L. E. HARRIS
JOANNE FENDELL

AUGUST 1983

U.S. ARMY ARMAMENT RESEARCH AND DEVELOPMENT CENTER
LARGE CALIBER WEAPON SYSTEMS LABORATORY
DOVER, NEW JERSEY

APPROVED FOR PUBLIC RELEASE; DISTRIBUTION UNLIMITED.

The views, opinions, and/or findings contained in this report are those of the author(s) and should not be construed as an official Department of the Army position, policy, or decision, unless so designated by other documentation.

The citation in this report of the names of commercial firms or commercially available products or services does not constitute official endorsement by or approval of the U.S. Government.

Destroy this report when no longer needed. Do not return to the originator.

REPORT DOCUMENTATION PAGE

READ INSTRUCTIONS BEFORE COMPLETING FORM

1. REPORT NUMBER: Technical Report ARLCD-TR-83033
2. GOVT ACCESSION NO.:
3. RECIPIENT'S CATALOG NUMBER:

4. TITLE (and Subtitle): N(2) AND CO VIBRATIONAL CARS AND H(2) ROTATIONAL CARS SPECTROSCOPY OF CH(4)-N(2)O FLAMES

5. TYPE OF REPORT & PERIOD COVERED: Final

6. PERFORMING ORG. REPORT NUMBER:

7. AUTHOR(s): Kenneth Aron, L. E. Harris, Joanne Fendell

8. CONTRACT OR GRANT NUMBER(s):

9. PERFORMING ORGANIZATION NAME AND ADDRESS:
ARDC, LCWSL
Applied Science Div [DRSMC-LCA-G(D)]
Dover, NJ 07801

10. PROGRAM ELEMENT, PROJECT, TASK AREA & WORK UNIT NUMBERS: 1L16122AH60

11. CONTROLLING OFFICE NAME AND ADDRESS:
ARDC, TSD
STINFO Div [DRSMC-TSS(D)]
Dover, NJ 07801

12. REPORT DATE: August 1983

13. NUMBER OF PAGES: 36

14. MONITORING AGENCY NAME & ADDRESS (if different from Controlling Office):

15. SECURITY CLASS. (of this report): UNCLASSIFIED

15a. DECLASSIFICATION/DOWNGRADING SCHEDULE:

16. DISTRIBUTION STATEMENT (of this Report):

Approved for public release; distribution unlimited.

17. DISTRIBUTION STATEMENT (of the abstract entered in Block 20, if different from Report):

18. SUPPLEMENTARY NOTES

Kenneth Aron, who co-authored this report, is associated with Geo-Centers, Inc., Newton, Massachusetts.

19. KEY WORDS (Continue on reverse side if necessary and identify by block number)

CARS
Nitrogen
Carbon monoxide
Hydrogen
Methane-nitrous oxide flame

20. ABSTRACT (Continue on reverse side if necessary and identify by block number)

Broadband CARS (coherent anti-Stokes Raman scattering) spectra of N(2) and CO were obtained from the post-flame gases of rich CH(4)-N(2)O flames by the use of the nonplanar BOXCARS technique. The temperature and concentration of both N(2) and CO in these flames, estimated from CARS spectra with the aid of model calculations, agreed with standard thermochemical predictions. In addition, several pure rotational H(2) CARS transitions, most of which had previously

(cont)

20. ABSTRACT (cont)

been unobserved, were seen in several spectral regions, most notably in both the CO and NO CARS regions. These observations are important in future modeling of CARS data.

CONTENTS

INTRODUCTION

Coherent anti-Stokes Raman scattering (CARS) spectroscopy has become an effective method for analysis and investigation of flames and combustion processes. The theoretical background of CARS and its experimental applications have been extensively reviewed (refs 1 through 6). CARS is based on the nonlinear response of a homogeneous medium upon which waves ω_1 and ω_2 are incident and which generates an oscillating polarization. The lowest order nonlinearity is the third order susceptibility, $\chi^{(3)}(-\omega_3, \omega_1, \omega_1, -\omega_2)$ which generates a frequency component of the polarization at $\omega_3 = 2\ \omega_1 - \omega_2$ by the process of three wave mixing (ref 7). Vibrational resonant enhancement of three-wave mixing occurs if $\omega_1 - \omega_2$ is made equal to a Raman active vibration, ω_v, in this way generating the CARS signal. Numerous flames have been studied with CARS of N_2, CO, H_2, and H_2O (refs 2 and 3).

Depending on the demands of the particular combustion circumstances to be studied, CARS can be carried out in several different modes. Normally ω_2 is narrowband and scanned to obtain the CARS spectrum at ω_3. However, to obtain spectra in transient or turbulent flames, it is appropriate to use a broadband ω_2 [approximately 150 cm^{-1} full width at half height (FWHH)] to obtain the full rovibrational spectrum at ω_3 within the time duration of the laser pulse (~10 ns) (ref 8).

The CARS experiments can also be carried out in different geometrical modes to effect the required phasematching for the coherent process. When ω_1 is split to achieve phasematching, it is termed BOXCARS (ref 9). In this case spatial resolution is improved since CARS generation occurs only where all three beams intersect. In folded (nonplanar) BOXCARS, there is the additional advantage that ω_3 is easily separated spatially from the generating beams (refs 10 and 11).

BOXCARS has been used to obtain temperature and concentration of post-flame gases in stationary flames using broadband (ref 12) and narrow band (ref 13) spectra, and in transient flames using single-shot (refs 14 and 15) spectra. Recently, broadband N_2 and N_2O CARS from the reaction zone of a flame has been reported utilizing the precisely defined spatial resolution of BOXCARS in the direction of the laser beams (ref 16). CARS allows direct monitoring of the rovibrational levels of the reactant molecules as they undergo flame reaction processes.

Because of these capabilities, measurement of N_2 and CO CARS was undertaken, particularly in rich CH_4/N_2O flames. It is seen that CARS-derived temperature and species concentrations agree with standard thermochemical estimates. In addition, pure rotational CARS signals were seen from several high-lying H_2 rotational levels, including two previously unobserved lines. The H_2 lines seen in this work lie in several spectral regions, most notably atop the CO CARS signal and in the region of the NO CARS transition. A thorough understanding of these H_2 lines would not only provide a new and uncomplicated approach to CARS temperature diagnostics, but would also clarify observed interferences in CARS spectra of hydrocarbon flames.

EXPERIMENTAL METHOD

The experimental method is described in references 16 and 17. Briefly, nonplanar BOXCARS was utilized to achieve phasematching. The output of a Quanta-Ray DCR-1A Nd/YAG laser at 1.06 microns (700 mJ) is doubled to generate the pump beam at 5320 Å (250 mJ) with a bandwidth of near 1 cm^{-1}. The pump beam is separated from the primary beam with prisms. The pump beam is split with a beam splitter to generate ω_{1p} and ω_{1s} and is used to pump a dye laser to generate the Stokes beam, ω_2. The dye laser consists of a flowing dye cell in a planar Fabry-Perot oscillator cavity pumped slightly off-axis by 20 percent of ω_{1s} with the output amplified by an additional dye cell pumped by the remainder of ω_{1s}. For the N_2 spectra, the dye laser was operated broadband with Exciton Rhodamine 640 in dry methanol at a concentration of 2.4×10^{-4} M and 3.2×10^{-5} M in the oscillator and amplifier dye cell, respectively, to produce 25 mJ ordinarily centered near 6060 Å (16502 cm^{-1}) with a bandwidth of 125 cm^{-1}. For the CO spectra, the pH of the oscillator dye solution was raised by the addition of methanol saturated with NaOH. For the investigation of the NO region, Exciton Kiton Red dye was used, 130 mg/L of dry methanol for the oscillator and 16 mg/L in the amplifier. To achieve BOXCARS geometry, ω_{1p} is again split with another beam splitter to generate ω_1 and ω_1'. In the optical configuration used to generate nonplanar BOXCARS, the ω_1, ω_1', and ω_2 beams are parallel and situated on a circle of 0.5-inch diameter at the focusing lens (200 mm focal length) with ω_1 and ω_1' in the central horizontal plane of the lens and ω_2 below ω_1 and ω_1' in the central vertical plane. Telescopes are inserted in the ω_{1p} and ω_2 beams to allow the focal spot size of both beams to be equalized. The telescopes also allow the position of the ω_1, ω_1', and ω_2 beamwaists to be adjusted such that they all intersect after focusing. This was achieved with 0.85x and 2x telescopes in ω_{1p} and ω_2, respectively.

To achieve phasematching, a 12.5 mm-thick optical flat, rotatable about its horizontal axis, was inserted into ω_2 before focusing. It was adjusted to maximize the ω_3 signal. The beams were recollimated with a 200 mm focal length lens, after which ω_3 was located below the plane of ω_1 and ω_1'. ω_1 and ω_2 were terminated with a neutral density filter. ω_3 was focused with a 50-mm focal length lens onto the slits of a 1/3-meter monochromator equipped with a 2,400 line/mm grating and a 25-micron slit. The signal was detected by a PAR SIT detector and processed by a PAR OMA2 system. Neon lines were used to calibrate the monochromator. The FWHM of the neon lines nearest ω_3 were determined to be nominally 2.0 to 3.5 cm^{-1} per channel, depending on the experiment.

Flame measurements were made on premixed CH_4/N_2O flames maintained on one of two circular burners. One burner was 1.8 cm in diameter and its surface was constructed of a matrix of steel syringe needles of 0.2 cm o.d. so that a flat flame could be obtained under suitable flow conditions. The second burner, of similar construction, consisted of two distinct sections: a 2.25-cm-diameter inner core area for the flame, constructed of 0.09-cm-o.d. needles and surrounded by a 1.0-cm-wide torus composed of 0.13-cm-o.d. needles through which argon could be flowed to provide an inert gas sheath for the flame. Matheson technical grade methane and chemically pure nitrous oxide were separately flowed through Matheson rotameters prior to premixing. The flow through the burner was adjusted according to equivalence ratio and the need for sufficient flow to prevent re-ignition

in the hotter flames. Equivalence ratio (ϕ) is defined here as the fuel/oxidant molar ratio divided by the stoichiometric fuel/oxidant molar ratio. For $\phi = 0.5$, the flow velocity was adjusted to 19.7 cm/s; for $\phi = 1.0$, 30.2 cm/s; for $\phi = 1.2$, 31.5 cm/s; $\phi = 1.8$, 16.2 cm/s; $\phi = 2.5$, 7.9 cm/s. The center line of the burner was placed at the intersection of the ω_1, ω_1', and ω_2 beamwaists. The burner was mounted on horizontal and vertical translation stages.

RESULTS

Broadband CO and N_2 spectra were obtained at several heights in 0.5, 1.0, 1.8, and 2.5 equivalence ratio flames. All these flames were scanned vertically along the center line, from a height of 2 mm to 60 mm above the burner surface. Spectra similar to those shown in figure 1 for N_2 and figure 2 for CO were obtained for $\phi = 1.0$, $\phi = 1.8$, and $\phi = 2.5$ flames at heights of 2 mm, 5 mm, 10 mm, 20 mm, 30 mm, 50 mm, and 60 mm.

The spectra shown in the figures and similar spectra taken at other positions in the flame allow the determination of temperature and concentration of N_2 and CO. N_2 CARS spectra were calculated with the method outlined in references 17, 18, and 19. The observed CARS spectrum is proportional to the square of the modulus of the third order susceptibility, $\chi^{(3)}$, which is the sum of a resonant term, χ_r, related to a nuclear displacement and a nonresonant term, χ_{nr}, related to electronic displacement:

$$\chi^{(3)} = \chi_r + \chi_{nr} \tag{1}$$

The resonant term is calculated as a sum of Lorentzian line shapes of each O(J) vibrational/rotational transition which is a function of the number density of the resonant molecule, the Raman cross-section, the Boltzman population difference, and the isolated linewidth. The calculated $|\chi^{(3)}|^2$ is first convoluted over the laser lineshapes and then over a triangular slit function. χ_r is the sum of a real χ_r', and an imaginary component, χ_r'', such that,

$$(\chi^{(3)})^2 = \chi'^2 + 2\chi'\chi_{nr} + \chi''^2 + \chi_{nr}^2 \tag{2}$$

χ' and χ'' display dispersive and resonant behavior, respectively, with respect to the detuning frequency, $\omega_i = \omega_j - (\omega_1 - \omega_2)$, where ω_j is the frequency of the Raman resonance. As the concentration of the resonant species is lowered, the cross term $\chi'\chi_{nr}$, which is dispersive, modulates the shape of the spectrum. The observation of dispersively modulated spectra allows estimation of the concentration in addition to the temperature based on model calculations. More critically, both temperature and concentration can be determined from these molecular spectra since in these hot flames the intensities of the higher hot bands of both CO and N_2 (particularly Q_{32} in both cases) are sufficiently concentration-dependent to allow both these variables to be modeled (ref 17). Observation of hot bands allows least-squares fitting of the calculated and experimental Q peaks maxima to give temperatures to ±100 K and concentration to ±10% absolute, based

on replicate determinations. The spectrum shown in figure 1 was obtained at 2 mm above the burner in an unshielded $\phi = 1.0$ flame. The temperature and concentration calculated for this flame were 3000 ± 100 K and 50% ± 5% N_2. The temperatures seemed to cool gradually, probing up the flame, with the N_2 concentration stable at 48% to 52%. At a height of 50 mm above the burner head, the temperature cooled only to about 2900 K. The temperature and concentration obtained from thermochemical calculations (ref 20)--2920 K and 51% N_2 for this flame--are within the error of the experimentally determined values.

In addition, to confirm the temperature and concentration measurements derived from N_2 CARS, measurements were taken with CO CARS in the same unshielded CH_4/N_2O flames. A CO CARS spectrum for a $\phi = 2.5$ shielded flame, shown in figure 2, is an example of CO CARS diagnostics. The CO CARS-derived data for the $\phi = 1.0$ flames (T = 3100 K, C = 8%) are consistent with the thermochemical data (T = 2920 K, C = 7.2% CO) and with the N_2 CARS data. However, for the $\phi = 2.5$ flame, shown in figure 2, the derived temperature and concentration values (T = 2550 K, C = 16% ± 1.6% CO) are actually hotter than the thermochemical data. This discrepancy for the rich $\phi = 2.5$ flames is discussed below. In summary, for the 1.0 flame, temperatures and concentrations were measured as 3100 K, 50% N_2 and 8% CO at 2.0 mm above the burner surface, cooling only slightly to 3000 K going up the flame even as high as 60 mm above the burner head. N_2 concentration increased only to 55% at 50-mm height, whereas by 20 mm above the burner, the CO signal had dropped below detection limits into the nonresonant background.

It was seen that for the $\phi = 1.8$ flame, both N_2 and CO CARS measurements approached the thermochemical predictions on species concentrations (CO = 16%, N_2 = 42%, T = 2734), even given the interaction of these rich flames with room air in this unshielded burner. At 2 mm above the burner head, N_2 CARS measured a temperature of 2600 K and 42% concentration. CO CARS, neglecting a sharp spike on the (1,0) CO peak, measured 2600 K and 8% CO. The N_2 concentration remained at 42% with a consistent temperature measurement near 2600 K even through the height of 60 mm. It was difficult to measure CO in this flame at heights greater than 30 mm above the burner.

CARS measurements on the $\phi = 2.5$ flame at 2 mm above the burner surface gave concentrations close to calculated (20%, CO, 35% N_2) but the observed temperatures, 2400 K to 2500 K, were somewhat hotter than calculated (2252 K) since the flame was, in fact, considerably leaner than 2.5 due to admixture with ambient O_2.

Except for use with rich flames such as the $\phi = 2.5$ flame, temperatures near to those which the calculations predict were seen in both of the burners which were used in these experiments. In fact, for the burner which was used only to compare shielded and unshielded flame behaviors, flames run at flows identical to those used with the first burner showed temperatures several hundred degrees below thermochemical predictions. At these flows, temperatures in this burner for $\phi = 1.8$ flames, for example, seemed to stabilize at 2300 to 2400 K. It is assumed that this burner exhibited substantial heat gain to its large burner head, necessitating the use of higher flow rates than used in the primary burner to raise the reaction zone.

During the course of obtaining the above temperature and concentration profiles for the various CH_4/N_2O flames with vibrational CARS spectra, several intense and narrow peaks were seen. These appeared in marked contrast to the broad rovibrational CO and N_2 transitions and exhibited a strong dependence on flame stoichiometry and, in at least one case, on the probed position within the flame.

The CARS spectrum in the CO spectral region of several CH_4/N_2O flames, ranging from a rich $\phi = 2.5$ flame to a $\phi = 1.2$ flame, is shown in figure 3. In these spectra, the (1,0), (2,1) and (3,2) vibrational bands of CO can be seen superimposed on the nonresonant CARS background. In addition, at $\Delta\nu = 2131$ cm^{-1}, superimposed on the (1,0) CO peak is a sharp peak whose linewidth seems to be instrument limited. This sharp "spike" dominates the spectrum for the fuel-rich flames and becomes less intense as the flame ratio approaches stoichiometric. The line intensity is not proportional to the square root of CO concentration, being more dependent than CO itself on flame stoichiometry. As is indicated above, reasonable agreement with thermochemical calculations for temperature and concentration of CO can be obtained only by attributing this peak to a species other than CO, with its position atop the CO (1,0) peak fortuitous.

In fact, this 2131 cm^{-1} peak has previously been observed (refs 21, 22, and 23). Klick et al (ref 23) attribute it to an (11,9) pure rotational transition of ground state H_2. Its behavior with respect to flame stoichiometry (and thus directly, with H_2 concentration) is documented below.

The CARS spectrum in the NO spectral region of several CH_4/N_2O flames, ranging here from a rich $\phi = 2.5$ flame to a lean $\phi = 0.5$ flame, is shown in figure 4. In none of the spectra was NO itself seen, but superimposed on the background nonresonant CARS signal were two narrow (linewidth limited by instrument resolution) peaks. The higher energy peak, at $\Delta\nu = 1809$ cm^{-1}, behaves similarly to the peak seen in the CO region: it is very intense in the rich flames and decreases in intensity as the flame is made leaner. The normalized intensity behavior which is nearly proportional to the square root of H_2 concentration is tabulated and compared in table 1. The $\Delta\nu = 1714$ cm^{-1} peak maintains a nearly constant normalized intensity relative to the nonresonant signal independent of flame stoichiometry. As discussed below, these peaks are also assigned as due to pure rotational H_2 CARS.

The signal from these narrow peaks was more intense in the NO region than in the CO region. That these peaks result from a CARS signal is obvious from the clear, typical CARS modulation seen in the $\Delta\nu = 1809$ cm^{-1} narrow peak in every spectrum in the NO region. Even in the $\phi = 0.5$ flame, where the peak itself is almost diminished into the noise, the typical CARS modulation is still apparent. This modulation on the H_2 peak cannot be seen as readily in the CO region, though on closer inspection and comparison of the different stoichiometric spectra, it can be discerned in this region as well.

In addition, because of the critical role N_2 CARS plays in flame temperature and concentration diagnostics, it is important to point out the possible observation of a narrow peak at 2298 cm^{-1}, almost centered atop the N_2 (2,1) hot band. Though such narrow structure is characteristic of N_2 CARS in hot flames, where

intensity enhancement due to overlap between a high V'' = 0 to v' = 1 rotational transition and a low v'' = 1 to v' = 2 rotational transition is predicted (ref 18), the persistence and high intensity of this narrow peak above the theoretical low-resolution plots in several spectra should not be overlooked. N_2 is the most commonly employed molecule in CARS diagnostics, and in these diagnostics the (1,0): (2,1) intensity ratio is critical for temperature and even concentration determinations. Any interference in the (2,1) peak intensity by a second species might consequently make erroneous any temperature/concentration measurements based on the (2,1): (1,0) N_2 ratio if its presence were not accounted for.

The possibility of a transition occurring at $\Delta\nu$ = 2298.5 cm^{-1} transition is the most difficult to fully assess. Because of its low intensity, and because of the clear J-structure of the N_2 vibrational bands, this line could be mistaken for N_2 rotational structure. Figures 5 and 6 show two spectra of N_2 of a ϕ = 1.8 flame at an experimental and calculated resolution of 2.0 cm^{-1} as well as a matching spectrum for each calculated with a resolution of 1.0 cm^{-1}. (The ω_2 profiles for these two spectra were quite different.) Figure 5 is calculated at 2400 K, 36%, while figure 6 is calculated with 2300 K, 37.5% N_2. It is seen that a sharp peak stands out above the unresolved rotational structure in the 2.0 cm^{-1} resolution case in the former examples, though it is not as evident in the latter example and is masked altogether in the high resolution plots and could be mistaken for a strong J-line or a superposition of several J-lines. High resolution (better than 0.1 cm^{-1}) calculations can be performed for N_2 at several temperature/concentration combinations, and at no reasonable set of conditions does only one rotational line near 2298.5 cm^{-1} or only one superposition of rotational lines show a marked intensity enhancement over all the other lines or superposition of lines. The (2,1) band itself actually appears as a double peak even at low resolution; at higher resolution, the prominent rotational lines and combinations which contribute to that double-headed structure are obvious. But even after the low resolution of the experiment conceals the other rotational structure, a narrow peak is still apparent. As seen in figure 7, this is even more marked in the untreated data. From energy level calculations, at 2298.5 cm^{-1} this narrow line is accidentally degenerate with one of the most intense combinations of rotational lines in the region of the (2,1) N_2 hot band transition for the flame conditions tested.

It was also important in these experiments to determine the effect of an argon shield on the flames which were tested. With the second burner, the most obvious result of flowing argon through the torus surrounding the flame was to effectively create a Smithells separator, even to the naked eye separating the inner and outer cones of the flame. That is, the argon flow prevented the infusion of room air into the flame until about 60 mm upstream, effectively lifting the outer cone or the outer diffusion flame where the excess oxidizable constituents would otherwise burn in air. This is borne out in the derived CARS data for both N_2 and CO in both ϕ = 2.5 and ϕ = 1.8 flames. Just above the burner head, before room air can mix with the flame in even the unshielded case, both the shielded and unshielded flames exhibit essentially the same temperature and concentration, 2250 K, 12% CO, 50% N_2 for ϕ = 2.5; 2500 K, 12% CO, 45% N_2, for ϕ = 1.8. Along the center line, this behavior is seen up to a height above the burner head of 10 mm. Above this height, for the unshielded burner, room oxygen

apparently mixes with these rich flames to produce a flame hotter than the shielded flame, with increased N_2 and decreased CO concentrations going up the center line. For $\phi = 2.5$ flames in the unshielded burner, the CO concentration drops to 7% at 2550 K at 10 mm height. Under identical conditions but with the added argon shield, flame analysis yields CO temperature = 2000 K and a CO concentration of 12%. By 30 mm, CO concentration drops below our detection limit in the unshielded flame, while in the shielded flame the CO concentration is maintained above 10% through a height of at least 60 mm. These differences are only somewhat less marked for the $\phi = 1.8$ flame. With this insight, experimentation was carried through predominantly on the unshielded flames.

DISCUSSION

CARS measurements were carried out on two different burners. In the first burner, which had no capability for shielding the flame, temperature and concentration were obtained from both N_2 and CO to characterize the post flame region of the $\phi = 1.0$, 1.8, and 2.5 flames. The second burner, which could be run with or without an argon shield, was used only to compare shielded with unshielded flame characteristics.

Using the first burner, in each of the $\phi = 1.0$, 1.8, and 2.5 flames, N_2 and CO temperatures were consistent to within ± 100 K, the estimated experimental error. In the $\phi = 1.0$ flame, the concentration of both N_2 and CO are in agreement within experimental error with the results of thermochemical calculations (ref 20). Agreement with the thermochemical calculations is attained by adjusting the flow to displace the reaction zone above the burner surface such that heat loss is minimized without inducing turbulent effects. In the $\phi = 1.8$ flame, agreement of the temperature with the thermochemical calculations cannot be expected since room air will enter into the flame reactions. This is even more marked in the still richer $\phi = 2.5$ flame. For the $\phi = 1.0$ and 1.8 flames, the measured temperatures are slightly lower than the calculated temperatures (the rich $\phi = 2.5$ flame measures with CARS hotter than thermochemical calculations predict) while the concentrations of both N_2 and CO along the centerline are close to their equilibrium values. These measurements serve to characterize the post-flame conditions under which the narrow resonances at $\Delta\nu = 2131$ cm^{-1} in the CO CARS region, and at $\Delta\nu = 1809$ cm^{-1} and $\Delta\nu = 1714$ cm^{-1} were observed.

Isolated narrow peaks, which appeared in marked contrast to the typical broad rovibrational spectra, were seen in several frequency ranges. The peaks at 1809 cm^{-1} and at 2131 cm^{-1} were the most prominent, and efforts at identification and documentation of behavior concentrated on these. To characterize these peaks, spectra were taken at $\phi = 0.5$, 1.0, 1.2, 1.8, 2.5, and 3.0. The normalized intensities of the transitions at 2131 cm^{-1} and at 1809 cm^{-1}, given in table 1, increased in going to richer flames nearly in proportion to the square root of the increase in the H_2 concentration obtained from the thermochemical calculations (also listed in table 1). The ratio of the intensities of the two transitions was nearly constant. The peak at 2131 cm^{-1} had previously been observed (refs 21, 22, and 23) and attributed to H_2 (ref 22), so it was sensible to investigate whether all the narrow peaks were due to pure rotational H_2 CARS. The

positions of the pure rotational transitions were calculated from the spectroscopic constants of Fink et al (ref 24). These constants closely fit the first four H_2 rotational lines observed by Stoicheff (ref 25) in the photographic Raman at room temperature. Higher rotational H_2 levels are not known to have been reported. Rotational levels in the ground vibrational state are calculated at 1816.8 cm^{-1} for the (9,7) S-transition [here, as will be the notation for all the S-type pure rotational transitions, of the form (J', J'')] and 2133.3 cm^{-1} for the (11,9) S-transition (the latter, as had previously been assigned). These are in close agreement with the observed transitions at 1809 cm^{-1} and 2131 cm^{-1}. In addition, in the first excited vibrational state of H_2, the (9,7) S-type rotational transition is calculated at 1720.8 cm^{-1} in agreement with the observed transition at 1714 cm^{-1}. The lower ratios of the normalized intensity of the 1809 cm^{-1} transitions, relative to the 2131 cm^{-1} transition for the ϕ = 1.8 and 2.5 flames, reflect the lower temperature in these flames. The temperatures in the ϕ = 1.8 and 2.5 flames are similar in the unshielded burner due to the effect of room air on the flame reactions. The relative constancy of the normalized intensity of the 1714 cm^{-1} peak may be due to the decrease of the first excited vibrational state population with lowering temperature as H_2 concentration increases with increasing ϕ.

The narrow peak observed in several spectra at $\Delta\nu$ = 2298.5 cm^{-1} cannot be correlated with an H_2 transition. Using these constants, the (10, 12) H_2 S-rotational (ground state vibrational level) transition is predicted to lie at 2288.8 cm^{-1} in the vicinity of the N_2 (v' = 2, v'' 1) hot band, approximately 10 cm^{-1} from the observed peak. This line would be more difficult to find than the other H_2 S-rotational transitions. The intensity of the N_2 signal from these flames would be expected to swamp the H_2 (10,12) S-rotational line but this line would appear still less intense than the other H_2 rotational lines for two other reasons as well. First, the nuclear statistics for the H_2 molecule result in a threefold decrease in the populations of the even H_2 rotational levels with respect to the odd levels. Second, from a simple Boltzman analysis, the population of the v'' = 10 level would be diminished by a further factor of 1.7 with respect to the v'' = 9 level at 2500 K relative to the (11,9) S-transition. Since intensity varies as the square of the population in CARS, this line would be expected to be perhaps 5% of the intensity of the stronger H_2 lines. As is explained below, it would be difficult to detect this line unless it were fortuitous enhanced by an energy degeneracy with N_2 rotational lines, which would be possible at these flame temperatures throughout the N_2 CARS region.

Even at only moderate resolutions, the (2,1) N_2 vibrational band, in calculated spectra, appears with marked structure, often double-headed (ref 17). This structure at these flame temperatures is due not only to the general crowding of rotational O-transitions from high-lying rotational levels of v'' = 0 with transitions from lower J-levels of v'' = 1, but also in particular to the degeneracy of certain of these N_2 transitions. Specifically, the (v'' = 0, J'' = 48) and the (v'' = 1, J'' = 26) N_2 Q-lines at $\Delta\nu$ = 2289.01 cm^{-1} are separated by 0.007 cm^{-1}, and the (0,42) and (1,12) Q-transitions near $\Delta\nu$ = 2298.54 cm^{-1} are separated by 0.30 cm^{-1}. Even at 1.0 cm^{-1} resolution, these near degeneracies show up as apparently enhanced, single-rotational transitions above the remainder of the more regular rotational structure. The narrow peak possibly observed in these

experiments appears at our resolution to be accidentally degenerate with the higher energy pair of these N_2 lines. It is this degeneracy which creates the difficulty in establishing a definitive observation of this narrow peak. If this peak is due to the presence of a second species and not to some error in the calculated fits, there is a triple enhancement of intensity in a narrow frequency range between a second species transition and N_2 rovibrational CARS transitions.

As seen in figures 5 and 6 which show two $\phi = 1.8$ spectra of resolution = 2.0 cm^{-1} and matching calculated spectra of resolution 1.0 cm^{-1} at T = 2400 K, C = 36% N_2 in figure 5 and T = 2300 K, C = 37.5% for figure 6, it is difficult to design reasonable conditions which would account for the enhanced intensity of the spike near 2898 cm^{-1} without suggesting the possibility of a contribution by a species other than N_2. There is no apparent reason why any one or few adjacent (or overlapped) N_2 rovibrational lines in that region--either from v'' = 0 or from v'' = 1-- would show such anomalous intensity that only one strong spike would appear even above the smooth unresolved rotational envelope at the 2.0 cm^{-1} resolution in several different observations. Nor is there any particular crowding of rotational lines in a limited frequency region, except the near degeneracies mentioned above.

Figure 7 shows a spectrum in a $\phi = 1.8$ flame (taken broadband with a single laser dye) showing CARS signals from N_2, CO, and H_2. Averaging out the irregularity in the N_2 (2,1) band, N_2 and CO CARS calculated using this spectrum give consistent measurements on this flame, with CO CARS giving a CO concentration of 13%, N_2 CARS showing 39% N_2, a CO-CARS-derived temperature = 2500 K and a N_2-derived CARS temperature = 2450 K, all consistent with thermochemical calculations.

CONCLUSION

For rich CH_4/N_2O flames, N_2- and CO-CARS provide species-to-species confirmation of experimentally-derived flame temperature/concentration data. Moreover, observation of previously unobserved H_2 rotational lines in a wide range of frequencies might provide additional third-species confirmations as well as a direct probe of flame temperatures and concentrations by a simple readout of narrow rotational line intensity ratios (with the proper dye intensity correction factor). For quick order of magnitude calculations, this might be a satisfactory adjunct to the current method of calculating complete rovibrational molecular spectra to determine flame temperature and concentration.

REFERENCES

1. R. L. Farrow, P. L. Mattern, and L. A. Rahn, "Comparison Between CARS and Corrected Thermocouple Temperature Measurements in a Diffusion Flame," Applied Optics, vol 21, 1982, p 3119.

2. R. J. Hall and A. C. Eckbreth, Optical Engineer, vol 20, 1981, p 494.

3. R. J. Hall and A. C. Eckbreth, "Coherent Anti-Stokes Raman Spectroscopy: Application to Combustion Diagnostics," Laser Applications, vol 5, R. K. Erf, Ed., Academic Press, New York, 1982.

4. S. Druet and J. P. Taran, "Coherent Anti-Stokes Raman Spectroscopy," Chemical and Biological Applications of Lasers, C. B. Moore, Ed., Academic Press, New York, 1979.

5. J. W. Nibler and G. V. Knighten, "Coherent Anti-Stokes Raman Spectroscopy," Raman Spectroscopy of Gases and Liquids, A. Weber, Ed., Springer-Verlag, New York, 1979.

6. J. W. Nibler, W. M. Shaub, J. R. McDonald, and A. B. Harvey, "Coherent Anti-Stokes Raman Spectroscopy, Vibrational Spectra and Structure, vol 6, J. R. Durig, Ed., Elsevier, Amsterdam, 1977.

7. N. Bloembergen, Nonlinear Optics, W. A. Benjamin, New York, NY, 1965.

8. W. B. Roh, P. W. Schreiber, and J. P. E. Taran, "Single-Pulse Coherent Anti-Stokes Raman Scattering," Applied Physics Letters, vol 29, 1976, p 174.

9. A. C. Eckbreth, "BOXCARS: Crossed-Beam Phase-Matched CARS Generation in Gases," Applied Physics Letters, vol 32, 1978, p 421.

10. R. L. Farrow, P. L. Mattern, and L. A. Rahn, "Cost-Beam, Background-Free CARS Measurement in a Methane Diffusion Flame," Sandia Laboratories Report 80-8640, Livermore, CA, 1980.

11. J. A. Shirley, R. J. Hall, and A. C. Eckbreth, "Folded BOXCARS for Rotational Raman Studies," Optics Letters, vol 5, 1980, p 380.

12. A. C. Eckbreth and R. J. Hall, "CARS Concentration Sensitivity with and without Nonresonant Background Suppression," Combustion Science and Technology, vol 25, 1981, p 175.

13. K. Muller-Dethlefs, M. Pealat, and J. P. E. Taran, Ber. Bunsenges. Physical Chemistry, vol 85, 1981, p 803.

14. L. E. Harris and M. E. McIlwain, Combustion and Flame, vol 48, 1982, p 97.

15. L. E. Harris and M. E. McIlwain, "Coherent Anti-Stokes Raman Spectroscopy in Propellant Flames," Fast Reactions in Ener. Sys., C. Capellos and R. F. Walker, Ed., Reidel, Boston, MA, 1981.

16. L. E. Harris, "Broadband N_2 and N_2O CARS Spectra," Chemical Physics Letters, vol 93, 1982, p 335.

17. L. E. Harris, "CARS Spectra from Lean and Stoichiometric CH_4/N_2O Flames," Combustion and Flame, in press.

18. R. J. Hall, "CARS Spectra of Combustion Gases," Combustion and Flame, vol 35, 1979, p 47.

19. A. Owyoung and L. A. Rahn, "High Resolution Inverse Raman Spectroscopy in a Methane-Air Flame," Journal of Quantum Electronics, vol 15, 1979, p 25D.

20. S. Gordon and B. J. McBride, "Computer Program for Calculations of Complex Chemical Equilibrium Compositions, Rocket Performance, Incident and Reflected Shocks, and Chapman-Jouquet Detonations," NASA SP-273, 1976.

21. A. C. Eckbreth, P. A. Bonczyk, and J. A. Shirley, "Investigation of Saturated Laser Fluorescence and CARS Spectroscopic Techniques for Combustion Diagnosis," U.S. Environmental Protection Agency, Report EPA-600/7-78-104, Cincinnati, OH, June 1978.

22. L. A. Rahn, L. J. Zych, and P. L. Mattern, "Background-Free CARS Studies of Carbon Monoxide in a Flame," Optics Communication, vol 30, 1979, p 249.

23. D. Klick, K. A. Marko, and L. Rimai, "Broadband Single-Pulse CARS Spectra in a Fired Internal Combustion Engine," Applied Optics, vol 20, 1981, p 1178.

24. U. Fink, T. A. Wiggins, and D. H. Rank, "Frequency and Intensity Measurements on the Quadrupole Spectrum of Molecular Hydrogen," Journal Molecular Spectroscopy, vol 18, 1965, p 384.

25. B. P. Stoicheff, "High Resolution Raman Spectroscopy of Gases," Canadian Journal of Physics, vol 35, 1957, p 730.

Table 1. Variation of the intensity of hydrogen rotational transition with hydrogen concentration

Frequency (cm^{-1})	Equivalence ratio (0) =	Normalized intensity* 1.2	1.8	2.5
2131		0.37	0.74	1.20
1809		0.80	1.80	2.90
I2131/I1809		0.46	0.41	0.41
H_2 concentration (%)		5.6	16.7	31.6

* Normalized intensity = (I - Inr)/Inr

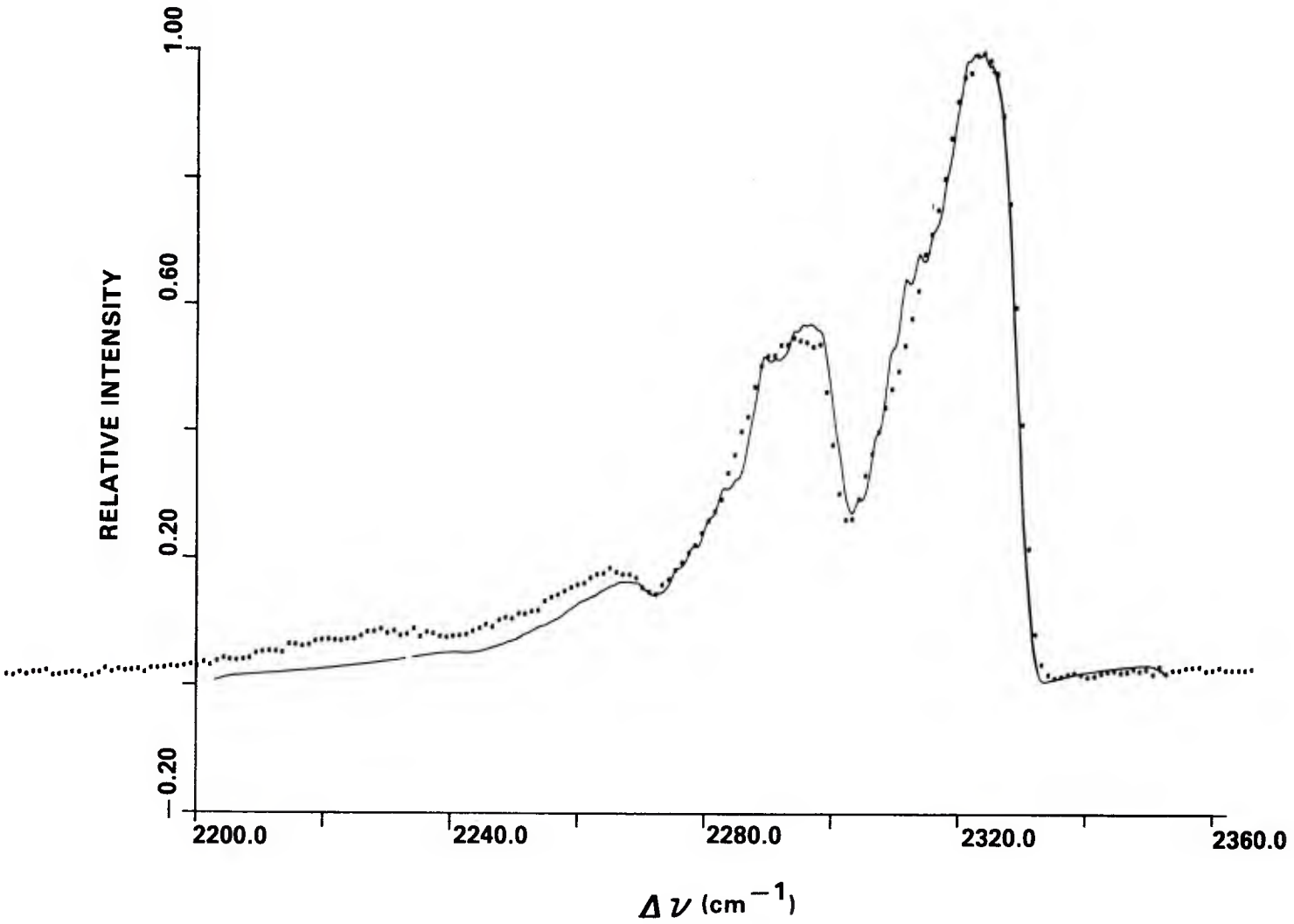

Figure 1. Experimental points and calculated spectrum (solid line) for N_2 CARS signal for a ϕ = 1.0 CH_4/N_2O flame, probe height = 2 mm; calculated variables used were T = 3000 K and concentration = 50%.

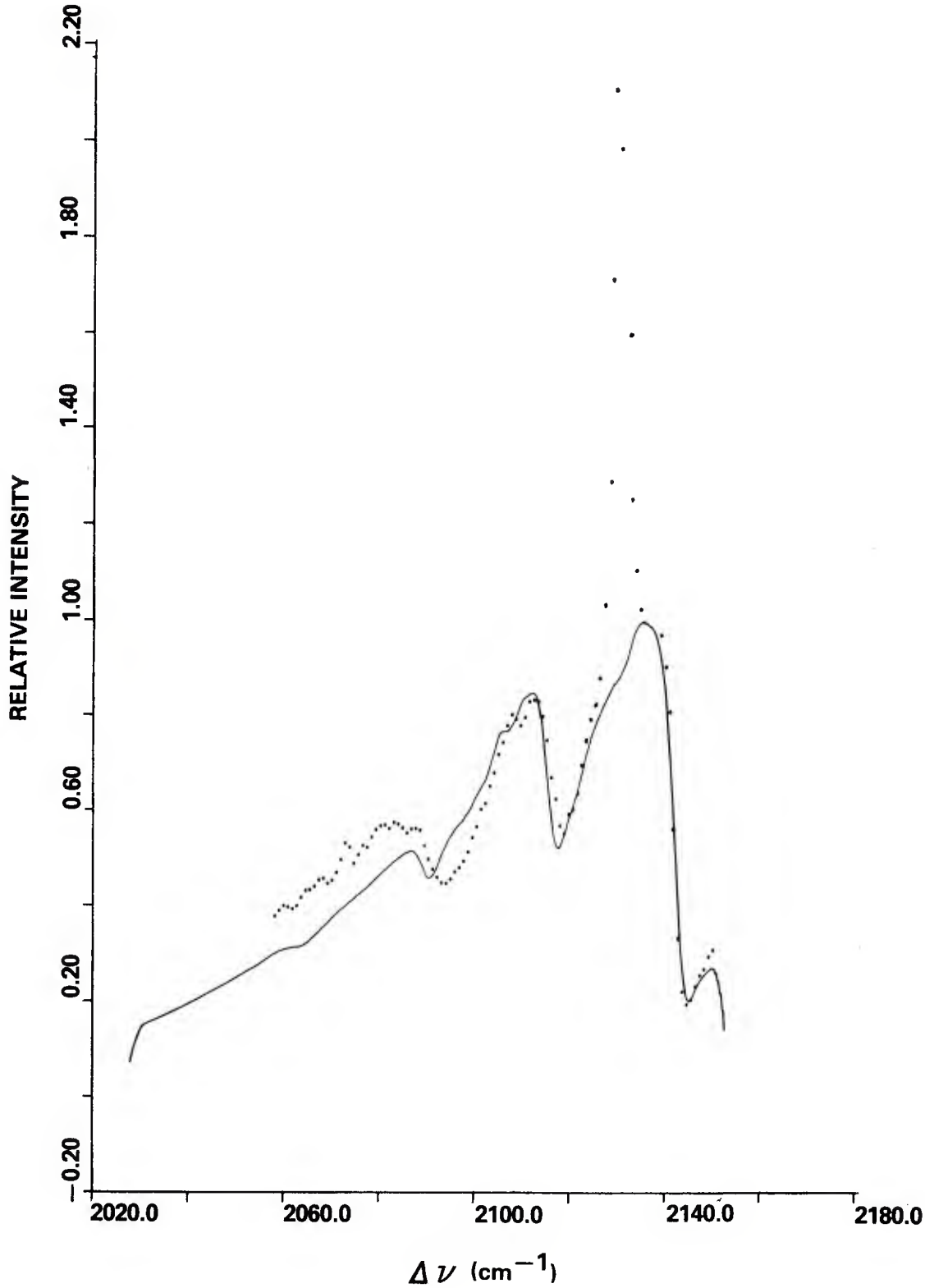

Figure 2. Experimental points and calculated spectrum (solid line) for a CO CARS signal for a ϕ = 2.5 CH_4/N_2O flame, probe height = 2 mm; calculated variables used were T = 2550 K and concentration = 16%.

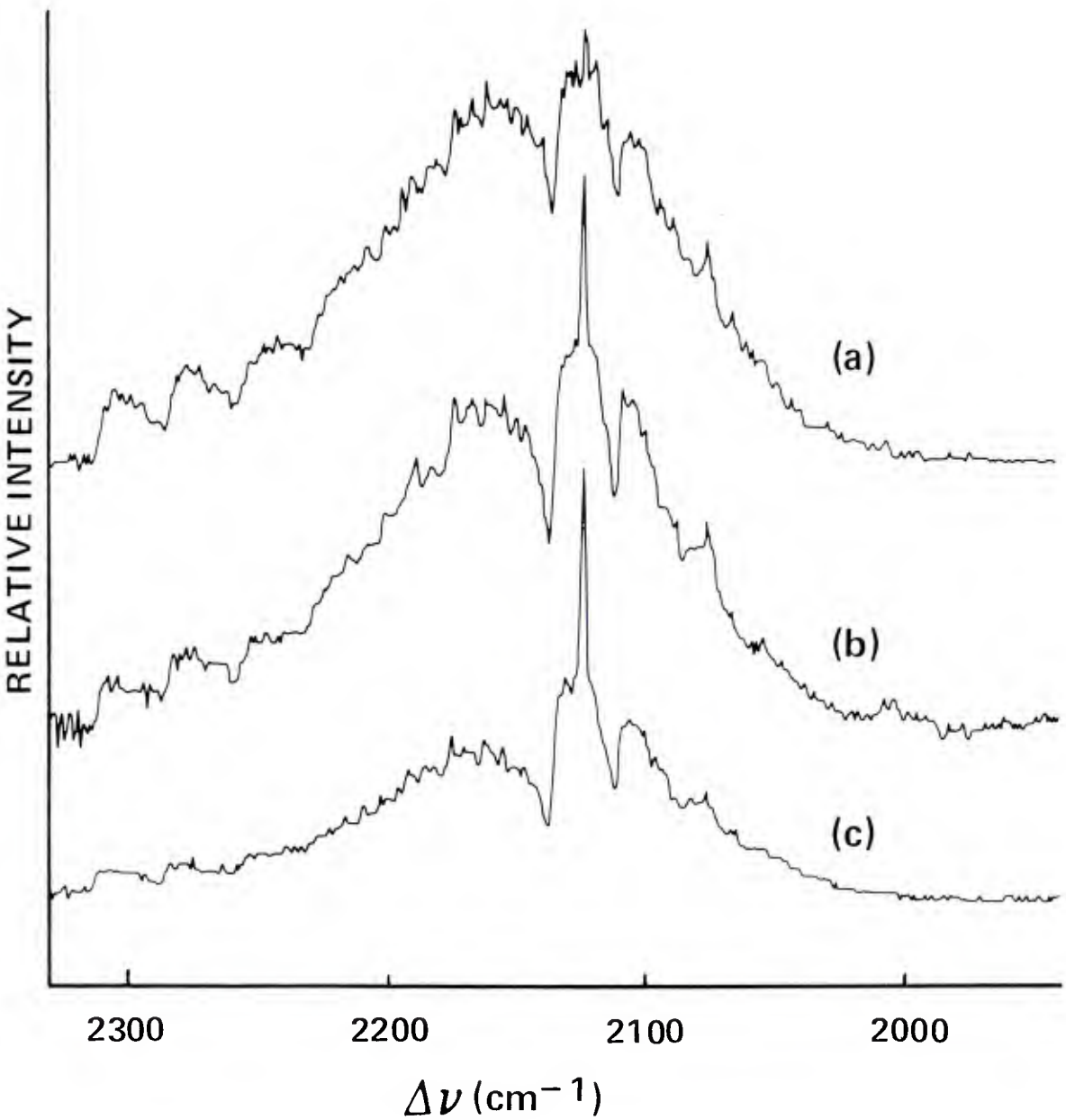

Figure 3. CARS spectrum in CO region for a (a) ϕ = 1.2 flame, (b) ϕ = 1.8 flame and (c) ϕ = 2.5 flame. The CO resonance is superimposed on the non-resonant susceptibility background. For analysis of the narrow peak at 2139 cm^{-1}, see text.

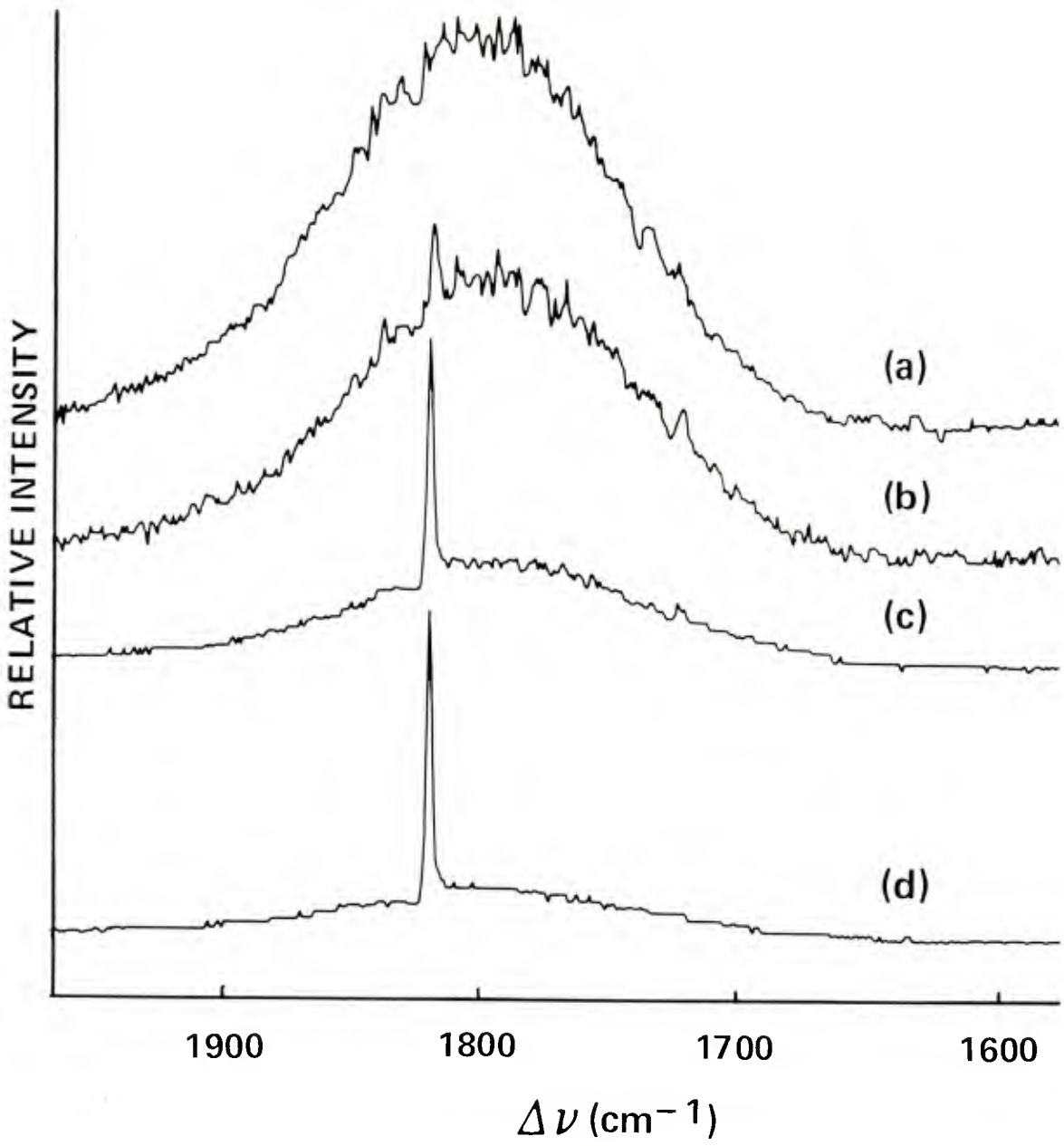

Figure 4. CARS spectrum showing behavior of narrow resonances from 1900 - 1600 cm^{-1}. Note intensity changes (superimposed on the background nonresonant susceptibility) for (a) $\phi = 0.5$, (b) $\phi = 1.2$, (c) $\phi = 1.8$ and (d) $\phi = 2.5$.

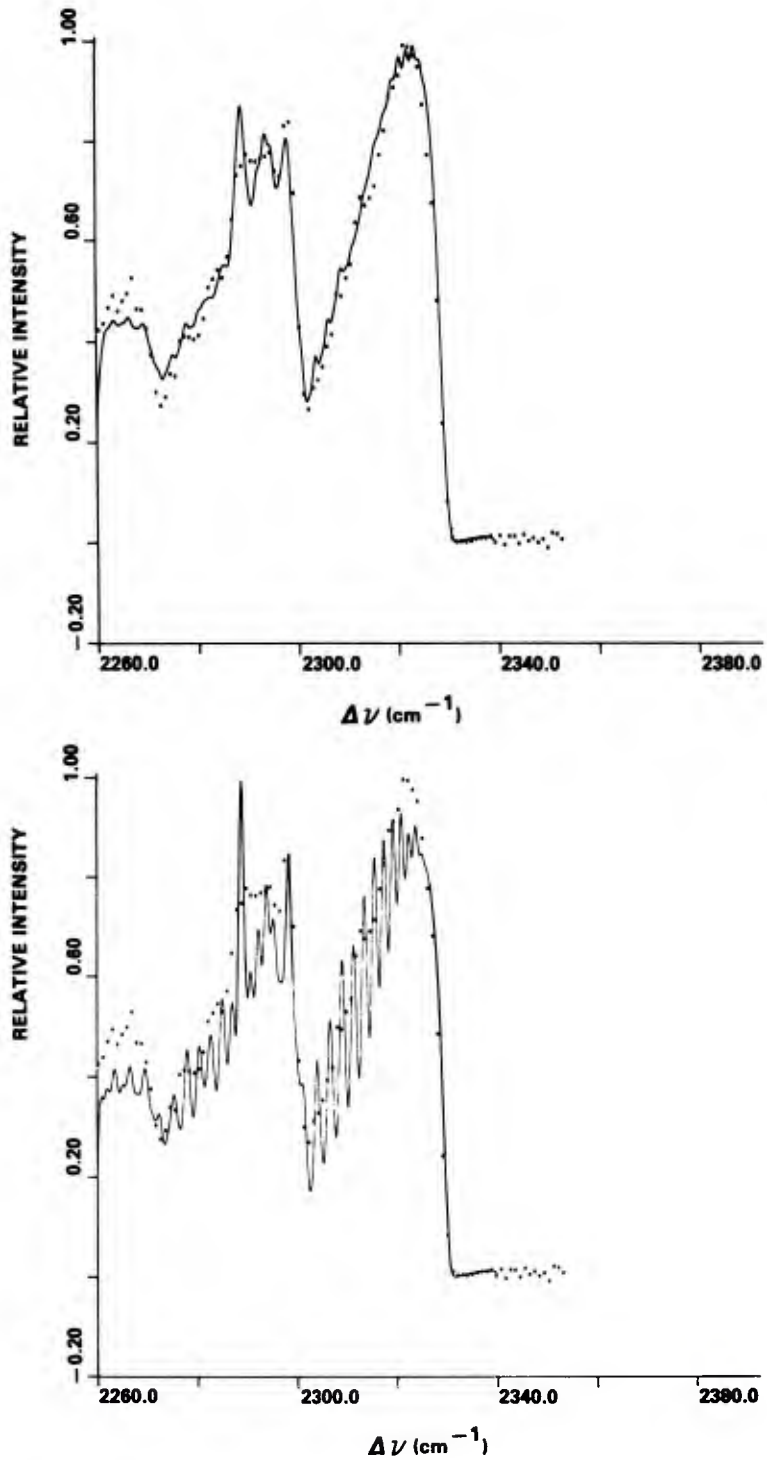

Figure 5. N_2 CARS spectrum in ϕ = 1.8 flames with calculated spectra of 2.0 and 1.0 cm^{-1} resolution; calculated parameters: T = 2400 K and C = 36%. Note experimental spike at 2298 cm^{-1}.

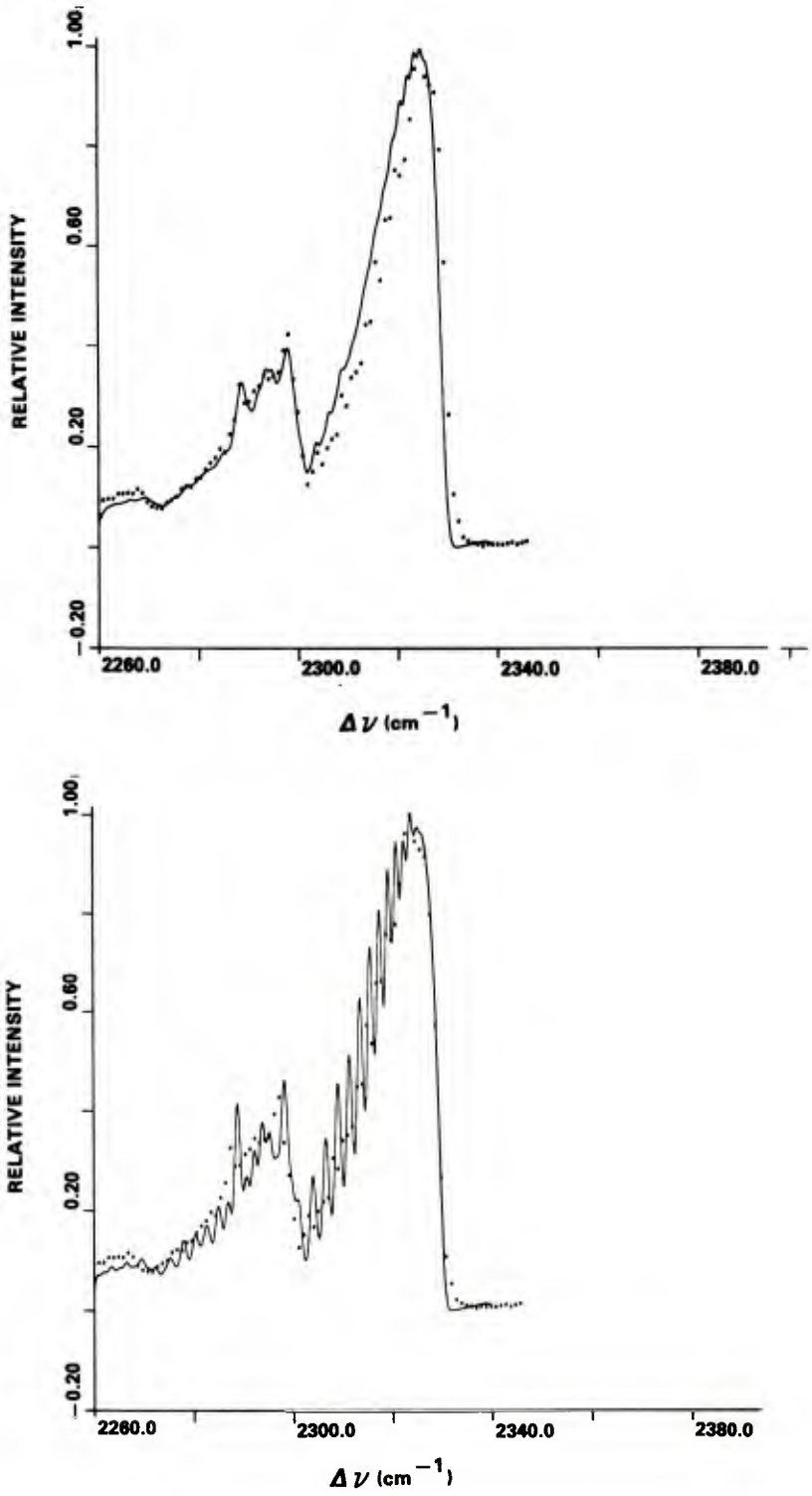

Figure 6. N_2 CARS spectrum in ϕ = 1.8 flames with calculated spectra 2.0 and 1.0 cm^{-1} resolution; calculated parameters: T = 2300 K and C = 37%. Note the experimental spike at 2298 cm^{-1}.

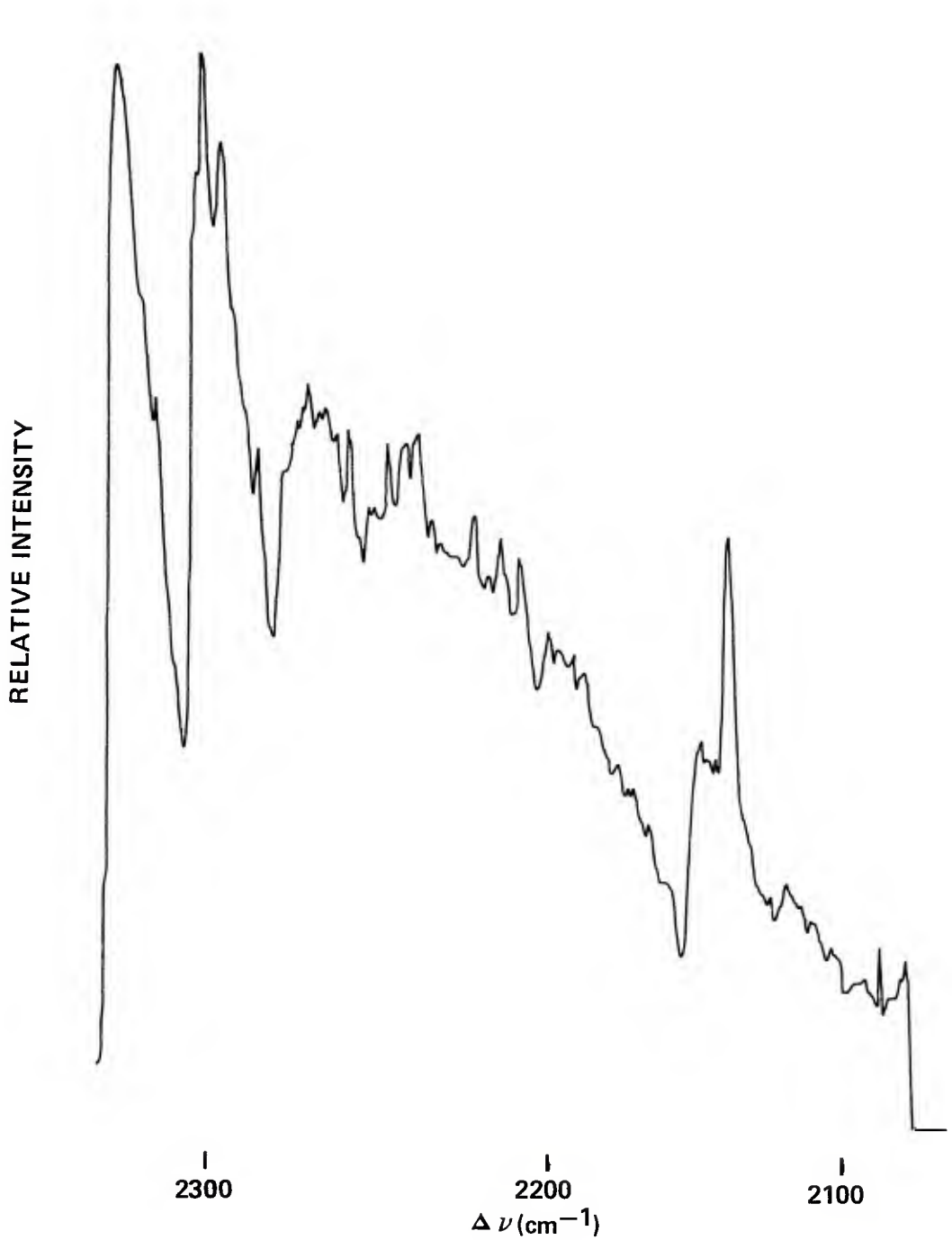

Figure 7. Unmodified spectrum in a ϕ = 1.8 flame showing signals from CO CARS, N_2 CARS and two H_2 CARS lines. Calculations on this spectrum show 39% N_2, 13% CO, 2500 K for CO temperature, 2500 K for N_2 temperature.

DISTRIBUTION LIST

Commander
Armament Research and Development Center
U.S. Army Armament, Munitions and
Chemical Command
ATTN: DRSMC-TSS(D) (5)
DRSMC-GCL(D)
DRSMC-LC(D), J. Frasier
J. P. Picard
DRSMC-LCA(D), A. Moss
DRSMC-LCA-G(D), J. Lannon
D. Downs
L. Harris (10)
T. Vladimiroff
A. Beardell
Y. Carignon
J. Fendell
K. Aron
E. Petro
DRSMC-LCE(D), R. Walker
P. Marinkas
C. Capellos
F. Owens
Dover, NJ 07801

Administrator
Defense Technical Information Center
ATTN: Accessions Division (12)
Cameron Station
Alexandria, VA 22314

Director
U.S. Army Materiel Systems
Analysis Activity
ATTN: DRXSY-MP
Aberdeen Proving Ground, MD 21005

Commander
Chemical Research and Development Center
U.S. Army Armament, Munitions and
Chemical Command
ATTN: DRSMC-CLJ-L(A)
DRSMC-CLB-PA(A)
APG, Edgewood Area, MD 21010

Director
Ballistics Research Laboratory
Armament Research and Development Center
U.S. Army Armament, Munitions and
Chemical Command
ATTN: DRSMC-TSB-S(A)
DRSMC-BLP(A), L. Watermier
A. Barrows
G. Adams
R. Fifer
M. Miller
T. Coffee
J. Heimeryl
C. Nelson
J. Vanderhoff
J. Anderson
Aberdeen Proving Ground, MD 21005

Chief
Benet Weapons Laboratory, LCWSL
Armament Research and Development Center
U.S. Army Armament, Munitions and
Chemical Command
ATTN: DRSMC-LCB-TL
Watervliet, NY 12189

Commander
U.S. Army Armament, Munitions and
Chemical Command
ATTN: DRSMC-LEP-L(R)
Rock Island, IL 61299

Director
U.S. Army TRADOC Systems
Analysis Activity
ATTN: ATAA-SL
White Sands Missile Range, NM 88002

Director
Defense Advanced Research Projects
Agency
ATTN: LTC C. Buck
1400 Wilson Boulevard
Arlington, VA 22209

Director
Institute for Defense Analyses
ATTN: H. Wolfhard
R. T. Oliver
400 Army-Navy Drive
Arlington, VA 22202

Commander
U.S. Army Materiel Development
and Readiness Command
ATTN: DRCDMD-ST
5001 Eisenhower Avenue
Alexandria, VA 22333

Commander
U.S. Army Watervliet Arsenal
ATTN: SARWV-RD, R. Thierry
Watervliet, NY 12189

Commander
U.S. Army Aviation Research
and Development Command
ATTN: DRSAV-E
P.O. Box 209
St. Louis, MO 63166

Director
U.S. Army Air Mobility Research
and Development Laboratory
Ames Research Center
Moffett Field, CA 94035

Commander
U.S. Army Communications Research
and Development Command
ATTN: DRDCO-PPA-SA
Fort Monmouth, NJ 07703

Commander
U.S. Army Electronics Research
and Development Command
Technical Support Activity
ATTN: DELSD-L
Fort Monmouth, NJ 07703

Commander
U.S. Army Missile Command
ATTN: DRSMI-R
DRSMI-YDL
Redstone Arsenal, AL 35809

Commander
U.S. Army Natick Research
and Development Command
ATTN: DRXRE, D. Sieling
Natick, MA 01762

Commander
U.S. Army Tank Automotive Research
and Development Command
ATTN: DRDTA-UL
Warren, MI 48090

Commander
U.S. Army White Sands Missile Range
ATTN: STEWS-VT
White Sands Missile Range, NM 88002

Commander
U.S. Army Materials and
Mechanics Research Center
ATTN: DRXMR-ATL
Watertown, MA 02172

Commander
U.S. Army Research Office
ATTN: Technical Library
D. Squire
F. Schmiedeshaff
R. Ghirardelli
M. Ciftan
P.O. Box 12211
Research Triangle Park, NC 27706

Office of Naval Research
ATTN: Code 473
G. Neece
800 N. Quincy Street
Arlington, VA 22217

Commander
Naval Sea Systems Command
ATTN: J. W. Murrin, SEA-62R2
National Center
Bldg 2, Room 6E08
Washington, DC 20362

Commander
Naval Surface Weapons Center
ATTN: Library Branch, DX-21
Dahlgren, VA 22448

Commander
Naval Surface Weapons Center
ATTN: Code 240, S. J. Jacobs, J. Sharma
Code 730
Silver Spring, MD 20910

Commander
Naval Underwater Systems Center
Energy Conversion Department
ATTN: Code 5B331, R. S. Lazar
Newport, RI 02840

Commander
Naval Weapons Center
ATTN: R. Derr
C. Thelen
China Lake, CA 93555

Commander
Naval Research Laboratory
ATTN: Code 6180
Washington, DC 20375

Superintendent
Naval Postgraduate School
ATTN: Technical Library
D. Netzer
A. Fuhs
Monterey, CA 93940

Commander
Naval Ordnance Station
ATTN: Dr. Charles Dale
Technical Library
Indian Head, MD 20640

AFOSR
ATTN: J. F. Masi
B. T. Wolfson
D. Ball
L. Caveny
Bolling AFB, DC 20332

AFRPL (DYSC)
ATTN: D. George
J. N. Levine
Edwards AFB, CA 93523

National Bureau of Standards
ATTN: J. Hastie
T. Kashiwagi
H. Semerjian
M. Jacox
K. Smyth
J. Stevenson
Washington, DC 20234

Lockheed Palo Alto Research Laboratories
ATTN: Technical Information Center
3521 Hanover Street
Palo Alto, CA 94304

Aerojet Solid Propulsion Co.
ATTN: P. Micheli
Sacramento, CA 95813

ARO Incorporated
ATTN: N. Dougherty
Arnold AFS, TN 37389

Atlantic Research Corporation
ATTN: M. K. King
5390 Cherokee Avenue
Alexandria, VA 22314

AVCO Corporation
AVCO Everett Research Laboratory
Division
ATTN: D. Stickler
2385 Revere Beach Parkway
Everett, MA 02149

Calspan Corporation
ATTN: E. B. Fisher
A. P. Trippe
P.O. Box 400
Buffalo, NY 14221

Foster Miller Associates, Inc.
ATTN: A. J. Erickson
135 Second Avenue
Waltham, MA 02154

General Electric Company
Armament Department
ATTN: M. J. Bulman
Lakeside Avenue
Burlington, VT 05402

General Electric Company
Flight Propulsion Division
ATTN: Technical Library
Cincinnati, OH 45215

Hercules Incorporated
Alleghany Ballistic Lab
ATTN: R. Miller
Technical Library
Cumberland, MD 21501

Hercules Incorporated
Bacchus Works
ATTN: B. Isom
Magna, UT 84044

IITRI
ATTN: M. J. Klein
10 West 35th Street
Chicago, IL 60615

Olin Corporation
Badger Army Ammunition Plant
ATTN: J. Ramnarace
Baraboo, WI 53913

Olin Corporation
New Haven Plant
ATTN: R. L. Cook
D. W. Riefler
275 Winchester Avenue
New Haven, CT 06504

Paul Gough Associates, Inc.
ATTN: P. S. Gough
P.O. Box 1614
Portsmouth, NH 03801

Physics International Company
2700 Merced Street
Leandro, CA 94577

Pulsepower Systems, Inc.
ATTN: L. C. Elmore
815 American Street
San Carlos, CA 94070

Rockwell International Corp.
Rocketdyne Division
ATTN: C. Obert
J. E. Flanagan
A. Axeworthy
6633 Canoga Avenue
Canoga Park, CA 91304

Rockwell International Corp.
Rocketdyne Division
ATTN: W. Haymes
Technical Library
McGregor, TX 76657

Pennsylvania State University
Department of Material Sciences
ATTN: H. Palmer
University Park, PA 16801

Princeton Combustion Research
Laboratories
ATTN: M. Summerfield
N. Messina
1041 U.S. Highway One North
Princeton, NJ 08540

Princeton University
Forrestal Campus
ATTN: I. Glassman
F. Dryer
Technical Library
P.O. Box 710
Princeton, NJ 08540

Purdue University
School of Mechanical Engineering
ATTN: J. Osborn
S. N. B. Murthy
N. M. Laurendeau
TSPC Chaffee Hall
W. Lafayette, IN 47906

Rutgers State University
Department of Mechanical and
Aerospace Engineering
ATTN: S. Temkin
University Heights Campus
New Brunswick, NJ 08903

SRI International
ATTN: Technical Library
D. Crosley
J. Barker
D. Golden
333 Ravenswood Avenue
Menlo Park, CA 94025

Stevens Institute of Technology
Davidson Library
ATTN: R. McAlevy, III
Hoboken, NJ 07030

United Technology
ATTN: Alan Ecbreth
Robert Hall
Research Center
East Hartford, CT 06108

Commander
Naval Research Laboratory
Chemistry Division
ATTN: A. Harvey
Washington, DC 20375

General Motors Research Laboratory
ATTN: J. H. Bechtel
Warren, Michigan 48090

System Research Laboratory
ATTN: L. Goss
2600 Indian Ripple Rd
Dayton, Ohio 45440

Exxon Research and Engineering
ATTN: A. Dean
M. Chou
P.O. Box 45
Linden, NJ 07036

Ford Motor Company
Research Staff
ATTN: K. Marko
L. Rimai
Dearborn, Michigan 48120

Sandia Laboratories
Applied Physics Division I
ATTN: L. Rahn
D. Stephenson
Livermore, CA 94550

Rensselaer Polytechnic Institute
Dept. of Chem. Engineering
ATTN: A. Fontijn
Troy, NY 12181

University of California,
San Diego
Ames Department
ATTN: F. Williams
P.O. Box 109
La Jolla, CA 92037

University of California
Dept. of Mechanical Eng.
ATTN: J. W. Daily
Berkeley, CA 94720

Univ. of Dayton
University of Dayton Research Inst.
Dayton, OH 45406

University of Florida
Dept. of Chemistry
ATTN: J. Winefordner
Gainesville, Florida 32601

University of Illinois
Dept. of Mechanical Eng.
ATTN: H. Krier
144 MEB, 1206 W. Green St.
Urbana, IL 61801

University of Minnesota
Dept. of Mechanical Eng.
ATTN: E. Fletcher
Minneapolis, MN 55455

University of California,
Santa Barbara
Quantum Institute
ATTN: K. Schofield
M. Steinberg
Santa Barbara, CA 93106

University of Southern California
Department of Chemistry
ATTN: S. Benson
Los Angeles, CA 90007

Stanford University
Department of Mech. Eng.
ATTN: R. Hanson
Stanford, CA 93106

University of Texas
Department of Chemistry
ATTN: W. Gardiner
H. Schaefer
Austin, TX 78712

University of Utah
Dept. of Chemical Engineering
ATTN: A. Baer
G. Flandro
Salt Lake City, UT 84112